# Caveolin-1 and Aquaporin-4 as Mediators of Fibrinogen-Driven Cerebrovascular Pathology in Hereditary Cerebral Amyloid Angiopathy

Vishal Singh[1], Nicholas Rochakim[1], Francesca Ferraresso[3,4,5], Arnab Choudhury[1], Christian J. Kastrup[3,6], Hyung Jin Ahn[1,2*]

1 Department of Pharmacology, Physiology and Neurosciences, Rutgers-New Jersey Medical School, Newark, NJ, USA

2 Brain Health Institute, Rutgers University, Piscataway, NJ, USA

3 Versiti Blood Research Institute, Milwaukee, WI

4 Michael Smith Laboratories, University of British Columbia, Vancouver, Canada

5 Department of Biochemistry and Molecular Biology, University of British Columbia, Vancouver, Canada

6 Departments of Surgery, Biochemistry, Biomedical Engineering, and Pharmacology and Toxicology, Medical College of Wisconsin, Milwaukee, WI

*Correspondence.

**Hyung Jin Ahn**

**Email:** hyungjin.ahn@rutgers.edu.

**Author Contributions:** V.S., C.J.K., and H.J.A. designed research; V.S., N.R., F.R., A.C., performed research; V.S., and H.J.A. analyzed data; and V.S., F.F., A.C., N.R., and H.J.A. wrote the paper.

**Competing Interest Statement:** The authors declare no competing interest.

**Keywords:** Fibrinogen, Cerebral amyloid angiopathy, Transcytosis, Caveolin-1, AQP4

## Abstract

Hereditary Cerebral Amyloid Angiopathy (HCAA) is a rare inherited form of CAA, characterized by increased vascular deposits of amyloid peptides. HCAA provides a unique opportunity to study the pathogenic mechanisms linked to CAA, as it is associated with severe cerebrovascular pathology. Some of HCAA-associated amyloid-β (Aβ) mutations significantly enhance the interaction between fibrinogen and Aβ, resulting in altered fibrin structure and co-deposition with Aβ in the perivascular space. However, the mechanisms underlying perivascular fibrinogen deposition and the associated cerebrovascular pathology in HCAA remain unclear. To investigate this, we analyzed TgSwDI transgenic mice carrying HCAA-associated mutations and observed a significant age-dependent increase in fibrin(ogen) extravasation and fibrin(ogen)-Aβ colocalization in the perivascular space. Moreover, Caveolin-1, a protein involved in non-specific transcytosis across the endothelium, significantly increased with age in TgSwDI mice and correlated with fibrin(ogen) extravasation. Additionally, we noted significant aquaporin-4 (AQP4) depolarization in the CAA-laden blood vessels of TgSwDI mice, which also correlated with fibrin(ogen) extravasation and fibrin(ogen)-Aβ colocalization. Given that AQP4 plays a crucial role in Aβ clearance via the glymphatic pathway, its depolarization may disrupt this critical clearance mechanism, thereby exacerbating CAA pathology. To further explore the relationship between fibrin(ogen) and these factors, we depleted fibrinogen in TgSwDI mice using siRNA against fibrinogen. This intervention resulted in decreased CAA, reduced caveolin-1 levels, attenuated microglial activation, restored polarized expression of AQP4, and improved spatial memory in fibrinogen-depleted TgSwDI mice. These findings suggest that targeting fibrinogen could be a promising strategy for mitigating CAA pathology and its associated cerebrovascular pathology.

## Main Text

## Introduction

Brain vascular changes have been reported as an early pathological event in Alzheimer's disease (AD) progression (1-4). Among these changes, cerebral amyloid angiopathy (CAA), characterized by the deposition of β-amyloid (Aβ) around cerebral blood vessels, plays a crucial role in vascular dysfunction in AD and is observed in over 80% of AD patients (5, 6). CAA contributes to a variety of vascular abnormalities, including altered cerebral blood flow, abnormal vascular reactivity, cerebral hemorrhages, and microinfarcts (7-10) all of which are linked to cognitive impairment in AD (11). While CAA most commonly occurs in a sporadic form in late-onset AD patients, hereditary forms of CAA (HCAA) present more severe CAA and cerebrovascular pathologies and typically manifest in midlife (12). The majority of HCAA cases are driven by variants of a single mutation in the amyloid precursor protein (APP), leading to a dramatic increase in CAA deposition within the brain (12). Clinically, HCAA is characterized by exacerbated CAA, recurrent hemorrhagic and/or ischemic strokes, progressive cognitive decline, neuroinflammation, and eventually, death (12-15). HCAA also exhibits significant cerebrovascular pathologies, such as blood-brain barrier (BBB) disruption, thickening of the vessel wall, and loss of vascular smooth muscle cells (16).

Both CAA and HCAA have some common clinical features such cerebral hemorrhages, microinfarcts, subcortical white matter lesions, and cognitive impairment (16, 17) and because HCAA is a familial form of CAA that exhibits more severe cerebrovascular pathology, HCAA offers a unique opportunity to explore the pathogenic mechanisms involved in CAA-linked cerebrovascular pathology. This is particularly valuable as it provides a genetic basis for developing animal models.

The Dutch mutation (E22Q) is the most prevalent form of HCAA-associated APP mutation. In addition, several other HCAA-related APP mutations, including the Iowa (D23N), Italian (E22K), and Flemish (A21G) variants, have been identified (16). Our recent study suggested a possible role of fibrinogen, primary protein component of blood clot in exacerbating CAA pathology. Amyloid-β (Aβ) peptides carrying Dutch or Iowa mutation bind strongly with fibrinogen compared to wildtype (WT) Aβ and severely altered fibrin structure and delayed fibrinolysis *in vitro*, which can lead to fibrin(ogen)/Aβ co-deposition in the occipital cortex of Dutch and Iowa HCAA patients (18). Fibrinogen has been implicated with AD pathogenesis by contributing to neurovascular damage, neuroinflammation, and neuronal degeneration (19-21). Additionally, mouse models bearing APP mutations associated with familial AD exhibit age-dependent fibrin deposition and abnormal cerebrovascular phenotypes (22, 23).

Despite several studies on the role of fibrinogen in CAA and AD pathogenesis, the mechanism underlying fibrinogen extravasation process and its role in cerebrovascular pathology in CAA remains unclear. Caveolae-mediated transcytosis may represent a potential mechanism for fibrinogen crossing the endothelial cells (ECs). Yang et al. found an age-related shift in BBB transport of plasma proteins from ligand-specific receptor-mediated to non-specific caveolar transcytosis (24). Caveolin-1 (Cav-1), a crucial structural protein component of caveolae, plays a significant role in regulating the transfer of molecules from blood to peripheral tissues by influencing caveolae formation (25). Furthermore, hyperfibrinogenemia has been linked to increased Cav-1 expression, and elevated levels of fibrinogen have been shown to enhance caveolae formation (26, 27).

Aquaporin-4 (AQP4) is the primary water channel in the cerebrovasculature (28) , predominantly localized to the perivascular astrocytic end-feet that envelop blood vessels (29, 30). AQP4 plays an important role in the clearance of solutes including Aβ by utilizing CSF and interstitial fluid flow through perivascular drainage (31, 32). Both A*qp4* gene deletion and mislocalization of AQP4 by *Snta1* knock-out, reduces down Aβ clearance and promotes vascular Aβ deposition (33-35).Several studies also described altered AQP4 expression and localization in AD and CAA patients (36-39). Loss of perivascular AQP4 impaired glymphatic exchange and promoted Aβ plaque formation in AD mice (40). AD patients also exhibit reduced perivascular AQP4 localization compared to cognitively normal individuals which is sufficient to impair CSF-ISF exchange and promote Aβ deposition, an early event in the AD pathological cascade (40). In AD mice lacking AQP4, a 55-65% decrease in Aβ clearance is observed as compared to AD mice with intact AQP4 functionality (41). Moreover, fibrinogen extravasation has been associated with AQP4 loss and dementia in the brains of Idiopathic normal pressure hydrocephalus (iNPH) patients, involving cerebrospinal fluid (CSF) disturbance (42).

Enhanced fibrinogen extravasation in cerebral cortex was significantly associated with elevated astrogliosis and with reduced expression of perivascular AQP4 in iNPH patients (42).

Given the lack of a clear mechanism behind fibrinogen extravasation and its role in exacerbating CAA pathology, we hypothesize that fibrin(ogen) extravasation is facilitated by an age-dependent increase in Cav-1 expression, resulting in the co-deposition of fibrin(ogen) and Aβ in the perivascular space. This, in turn, may trigger neuroinflammation and disrupt the localization of AQP4 in astrocyte end-feet. The loss of AQP4 polarization could impair glymphatic clearance of Aβ, further exacerbating CAA pathology and contributing to cognitive decline. This study aims to elucidate the mechanisms underlying these processes, providing new insights into the interplay between fibrinogen, AQP4, and cerebrovascular dysfunction in CAA and AD.

## Results

### *1) Age dependent increase of fibrin(ogen) extravasation and fibrin(ogen)-Aβ co-deposition in TgSwDI mice*

Our previous study found that increased interaction between HCAA-type mutant Aβs and fibrin(ogen) may not only result in severely altered fibrin structure and delayed fibrinolysis *in vitro* but can also lead to extensive fibrin(ogen)/Aβ co-deposition in HCAA patients (18). To further investigate the effect of HCAA mutations on fibrin(ogen) deposition *in vivo*, we analyzed fibrin(ogen) extravasation and the co-deposition of fibrin(ogen) with Aβ in TgSwDI mice, a transgenic mouse model of HCAA, and compared the findings with WT littermates. Additionally, we explored age-dependent changes in these pathological events to better understand the disease progression.

We analyzed fibrin(ogen) extravasation, CAA, and fibrin(ogen)-Aβ co-deposition in TgSwDI mice and WT littermates at 7, 12, and 18 months of age using immunohistochemistry. We observed significant CAA in thalamus of 7-months-old TgSwDI compared to WT littermates, with no change in cortex and hippocampus (SI Appendix Fig. 1A and B). However, we found a significant age-dependent increase of CAA in the hippocampus and thalamus of 12- and 18-months-old TgSwDI mice compared to WT littermates (Fig. 1A-D). At 7 months, there was no significant extravascular fibrin(ogen) deposition in any brain region of TgSwDI mice (SI Appendix Fig. 1A and C). However, we observed a significant. fibrin(ogen) extravasation in the hippocampus and thalamus of 12- and 18-months-old TgSwDI mice compared to WT littermates (Fig. 1A, B, E, F). Images of individual vessels clearly showed fibrin(ogen) extravasation and its co-deposition with Aβ in the perivascular space in hippocampus and thalamus of 12 and 18-months-old TgSwDI mice (Fig. 1B). Fibrin(ogen) was visibly extravasating from the vessel lumen into the brain parenchyma, with some remaining trapped within the vessel lumen (Fig. 1B). A significant increase in fibrin(ogen)-Aβ co-deposits was also observed in 12- and 18-months-old TgSwDI mice compared to respective WT littermates (Fig.1 A, B, G, H). Since the hippocampus and thalamus were the brain areas most affected by CAA and fibrin(ogen) extravasation, while the cortex

was less impacted in TgSwDI mice, we focused our study on these two regions for the rest of our study.

### *2) Blood brain barrier integrity is preserved in TgSwDI mice.*

Hemorrhagic strokes, vascular degeneration, and BBB leakages are pathological features observed in HCAA patients (43, 44). To explore these pathological features of HCAA in our study, we analyzed microhemorrhages and BBB integrity in 18-months-old TgSwDI mice and WT littermates. We hypothesized that microhemorrhages and BBB disruption are responsible for fibrin(ogen) extravasation in TgSwDI mice. To test this idea, we performed Prussian blue histology to detect accumulation of ferric iron, known to be present in microhemorrhage (45). However, our analysis revealed no significant difference in the number of microhemorrhages between TgSwDI and WT littermates at 18 months of age (SI Appendix Fig. S2A, B), consistent with findings from other research groups (46, 47). Furthermore, we investigated BBB integrity using Evans blue dye (EBD), which exhibits a strong affinity for albumin and its leakage into the brain parenchyma indicates BBB disruption (48, 49). Spectrophotometric analysis of brain homogenates from 18-months-old TgSwDI and WT littermates showed no significant differences in EBD content in the cortex and hippocampus (SI Appendix Fig. S2C). Additionally, we evaluated the expression of tight junction proteins, including claudin-5, occludin, and ZO-1, via western blotting. Our results indicated no discernible changes in the expression of these tight junction proteins between TgSwDI mice and WT littermates at 18 months of age (SI Appendix Fig. S2D - G). Overall, our findings showed that 18-months-old TgSwDI mice and WT littermates did not differ in microhemorrhage levels, BBB permeability, or tight junction protein expression. This suggests these factors may not contribute to fibrin(ogen) extravasation in this model.

### 3) *Caveolae-mediated transcytosis-related proteins are altered in an age-dependent manner in TgSwDI Mice.*

Given the preserved BBB integrity in TgSwDI mice, we sought to identify alternative molecular mechanisms that could facilitate the extravasation of fibrinogen across the BBB, leading to its deposition in the perivascular space. Recent study has found that an age-dependent increase in non-specific caveolae-mediated transcytosis facilitates BBB transport of circulatory plasma proteins (24). In absence of tight junction proteins dysfunction, Cav-1 plays a crucial role in compromising BBB permeability, allowing plasma proteins, to cross the BBB via caveolae-mediated transcytosis (50, 51). We hypothesized that Cav-1 levels could be increased in the brains of aged TgSwDI mice, facilitating to the transcytosis of fibrinogen across brain endothelial cells and its deposition in the perivascular space. To test this, we analyzed Cav-1 levels in endothelial cells by assessing their colocalization with CD31 (an endothelial cell marker) in TgSwDI mice and WT littermates in an age-dependent manner. We found that at 7-months of age, there was no significant difference in the endothelial Cav-1 expression between TgSwDI and WT littermates across brain regions analyzed (SI Appendix Fig. S3A and B). However, at both 12 and 18- months of age, TgSwDI mice showed significantly higher endothelial Cav-1 levels in the hippocampus and thalamus compared to WT littermates (Fig. 2A-C).

Major facilitator superfamily domain containing 2a (Mfsd2a) is a key negative regulator of caveolae-mediated transcytosis, essential for maintaining BBB integrity in the central nervous system (CNS) and is exclusively expressed in brain endothelial cells (52, 53). While no significant difference in endothelial Mfsd2a levels was observed between TgSwDI and WT littermates at 12 months of age, despite a strong tendency toward decreased Mfsd2a levels in the thalamus (Fig. 2D and E), Mfsd2a levels were significantly decreased in the hippocampus and thalamus of 18-months-old TgSwDI mice, with no notable changes in the cortex compared to WT littermates (Fig. 2D and F). The significant increase in endothelial Cav-1 levels and the corresponding decrease in Mfsd2a levels in the hippocampus and thalamus of aged TgSwDI mice suggest that these molecular changes may facilitate caveolae-mediated transcytosis, contributing to fibrinogen extravasation across the BBB. These findings implicate age-dependent dysregulation of Cav-1 and Mfsd2a in the hippocampus and thalamus as key drivers of BBB permeability, potentially exacerbating vascular pathology in TgSwDI mice.

*4) Perivascular AQP4 loss progresses with age and is associated with fibrin(ogen)-Aβ co-deposits in CAA pathology.*

Since fibrin(ogen)-Aβ co-deposits are localized in the perivascular space in both TgSwDI mice and HCAA patients (18), and increased levels of extravasated fibrin(ogen) are associated with reduced perivascular AQP4 in iNPH patients (42), we aimed to investigate whether this co-deposition affects perivascular AQP4 distribution, or if AQP4 depolarization primarily induces CAA formation, followed by fibrin(ogen) binding to the perivascular Aβ in TgSwDI mice. To achieve this goal, we conducted a comprehensive analysis of perivascular AQP4 levels in TgSwDI mice across different ages compared to WT littermates: 7 months (CAA present only in the thalamus), 12 months (CAA in both the hippocampus and thalamus), and 18 months (amplified CAA in the hippocampus and thalamus). Additionally, we compared perivascular AQP4 levels between CAA-laden vessels and non-CAA vessels (those without visible CAA pathology) in TgSwDI mice.

At 7 months of age, while there was a significant increase in CAA in the thalamus of TgSwDI mice (SI Appendix Fig. S1), there was no significant difference in perivascular AQP4 levels in the thalamus and other brain regions between TgSwDI and WT littermates (SI Appendix Fig.4A and B). By 12 and 18 months of age, TgSwDI mice exhibited a significant age-dependent decrease of perivascular AQP4 levels in both hippocampus and thalamus, but not in cortex compared to WT littermates (Fig. 3A-C). Additionally, perivascular AQP4 was significantly reduced in CAA-laden vessels within the hippocampus and thalamus compared to non-CAA vessels in 12- and 18-months-old TgSwDI mice (Fig. 3D and E). Interestingly, the loss of perivascular AQP4 in TgSwDI mice was accompanied by increased level of AQP4 outside blood vessels (non-vascular AQP4) (Fig. 3A), suggesting AQP4 depolarization. Taken together, our study showed that perivascular AQP4 levels in TgSwDI mice decreased significantly with age in regions affected by CAA, and AQP4 depolarization began after the onset of CAA, with greater reductions observed in CAA-laden vessels. Since the age and specific brain regions showing AQP4 depolarization coincide with fibrin(ogen)-Aβ co-deposits (Fig. 1), these observations suggest that the perivascular fibrin(ogen)-Aβ co-deposits may be associated with AQP4 depolarization, potentially exacerbating CAA pathology.

5) *Depletion of plasma fibrinogen decreases CAA and restores impaired spatial memory in TgSwDI mice.*

Since both previous studies and our current research suggest a potential association between fibrinogen extravasation, CAA, and CAA-related pathologies, we investigated the effects of fibrinogen depletion on these pathological features in TgSwDI mice. Ancrod, a defibrinogenating agent derived from the venom of the Malayan pit viper, has previously been reported to reduce fibrinogen-mediated pathology by lowering fibrinogen levels in the blood, thereby decreasing CAA pathology and improving memory in AD mice (54). However, clinical study for ischemic stroke showed that ancrod increased the risk of intracerebral hemorrhage, and its efficacy has not been clearly demonstrated, highlighting the need for alternative approaches (55). To address this, we utilized lipid nanoparticle (LNP)-encapsulated small interfering RNA (siRNA) specifically targeting the fibrinogen alpha chain (siFga) to deplete fibrinogen in the blood. This siRNA approach did not alter hemostasis (56) and has been used safely in various animal models, leading to robust and controllable depletion of plasma fibrinogen (57-59). In our study, we administered siRNA targeting luciferase (siLuc) as a negative control. For clarity and consistency throughout the manuscript, mice treated with siLuc will be referred to as siLuc WT or siLuc TgSwDI, and those treated with siFga will be designated as siFga WT or siFga TgSwDI.

Mice were sacrificed at 12-months of age following three months of treatment with siRNA LNPs. Western blot analysis confirmed the efficacy of siFga, showing a reduction in plasma fibrinogen levels by more than 90% compared to siLuc-treated mice (Fig. 4A and B). While siLuc TgSwDI mice exhibited significantly higher CAA in the hippocampus and thalamus compared to siLuc WT and siFga WT mice, a significant reduction in CAA was observed in the hippocampus and thalamus of siFga-treated TgSwDI mice compared to siLuc TgSwDI mice (Fig. 4C and D). We further analyzed whether fibrinogen depletion affected Aβ plaque pathology. Although siLuc TgSwDI mice showed increased Aβ plaques in the cortex, hippocampus, and thalamus, siFga treatment did not alter Aβ plaque levels in any of these brain regions in siFga TgSwDI mice (SI Appendix, Fig. S5A and B). These results suggest that fibrinogen depletion specifically reduces CAA pathology around blood vessels without affecting Aβ plaques in the brain parenchyma.

Since CAA is associated with cognitive decline and TgSwDI mice have been reported to exhibit spatial memory deficits, as assessed by the Barnes maze task (60-62), we tested whether fibrinogen depletion could improve spatial memory impairment in TgSwDI mice. Upon fibrinogen depletion, we found significant improvement in spatial memory in siFga TgSwDI mice compared to siLuc TgSwDI mice in Barnes maze task (Fig. 4 E and F). During the probe trial, the latency to find the target hole decreased significantly in siFga TgSwDI mice compared to siLuc TgSwDI mice, reaching levels similar to siLuc WT mice (Fig. 4E). Additionally, the cumulative duration spent in the target hole (TH) increased significantly in siFga TgSwDI mice compared to siLuc TgSwDI mice and was restored to levels comparable to siLuc WT (Fig. 4F). siFga WT mice showed similar spatial memory abilities as siLuc WT (Fig. 4E and F), indicating that fibrinogen depletion does not cause cognitive defects in WT mice. Overall, our results suggest that fibrinogen depletion reduces CAA and restore spatial memory in TgSwDI mice.

6) *Fibrinogen depletion mitigates microglial-mediated neuroinflammation in CAA affected regions of TgSwDI mice.*

Fibrinogen is known to activate microglia via the Mac-1 integrin receptor, where CD11b serves as the α chain of Mac-1 (63). Fibrinogen triggers rapid microglial responses toward the vasculature and plays a key role in axonal damage during neuroinflammation (64). Given fibrinogen is proinflammatory, and its colocalization with Aβ in the perivascular space contributes to persistent neuroinflammation, we investigated the impact of fibrinogen depletion on microglia mediated neuroinflammation in TgSwDI mice using siRNA LNPs

We used CD11b as marker of microglial cells and found a significant increase in the ameboid morphology of microglial cells, indicating an activated state, in cortex, hippocampus, and thalamus of siLuc TgSwDI compared to siLuc WT (Fig. 5A). In siFga TgSwDI mice, the levels of activated microglia were significantly reduced in the hippocampus and thalamus compared to siLuc TgSwDI, with no significant change in the cortex (Fig. 5B). Interestingly, the majority of activated microglia in the hippocampus and thalamus were located around CAA and blood vessels in siLuc TgSwDI mice, whereas in the cortex, most activated microglia were found surrounding Aβ plaques (Fig. 5A). This selective reduction in the hippocampus and thalamus could be attributed to the fact that fibrinogen depletion specifically targets CAA pathology around blood vessels, which is more pronounced in these regions. Since siFga treatment effectively reduced CAA in the hippocampus and thalamus but did not alter Aβ plaque levels in any brain region, the observed changes in microglial activation are likely related to the reduction in CAA rather than Aβ plaque pathology. In contrast, the cortex may not have experienced a similar reduction in activated microglia because the treatment did not significantly affect Aβ plaques, which are the primary drivers of microglial activation in that region. Based on this idea, we further analyzed the levels of activated microglia associated with blood vessels (vascular microglia) and found a significant increase in activated vascular microglia around CAA in the hippocampus and thalamus of siLuc TgSwDI mice compared to siLuc WT, with no such increase observed in the cortex (Fig. 5C). Treatment with siFga significantly decreased the activation of vascular microglia in both the hippocampus and thalamus compared to siLuc TgSwDI mice (Fig. 5C). Our results indicate that fibrinogen depletion specifically reduces vascular microglial activation around CAA in TgSwDI mice, where fibrinogen and Aβ are co-deposited.

7) *Fibrinogen depletion decreased Cav-1 levels and restored perivascular AQP4 localization in TgSwDI mice.*

A previous study reported that in a mouse model of hyperfibrinogenemia, a condition characterized by elevated plasma fibrinogen levels, Cav-1 expression and caveolae-mediated transcytosis are both increased (26). Therefore, we investigated the impact of fibrinogen depletion on Cav-1 expression in TgSwDI mice. We found that siFga-treated TgSwDI mice exhibited significantly lower Cav-1 expression in the hippocampus and thalamus compared to siLuc TgSwDI mice. As expected, siLuc TgSwDI showed significantly higher Cav-1 expression compared to siLuc WT in both regions (Fig. 6A and

B). These results suggest that reducing blood fibrinogen levels restores normal endothelial Cav-1 expression in TgSwDI mice.

Given the possibility that perivascular fibrin(ogen)-Aβ co-deposits may be associated with AQP4 depolarization (Fig. 3), we examined whether fibrinogen depletion, linked to a reduction in CAA, could restore perivascular AQP4 polarization in TgSwDI mice. Our results showed that siFga-treated TgSwDI mice exhibited significantly higher perivascular AQP4 levels in both the hippocampus and thalamus compared to siLuc TgSwDI mice, with levels similar to siLuc WT (Fig. 6C and D). In contrast, siLuc-treated TgSwDI mice exhibited significantly lower perivascular AQP4 levels compared to siLuc WT (Fig. 6C and D). Simultaneously, non-vascular AQP4 levels were significantly reduced in siFga TgSwDI mice compared to siLuc TgSwDI mice (Fig. 6C). These findings suggest that fibrinogen depletion can restore perivascular AQP4 levels in TgSwDI mice, which may further contribute to reducing CAA by enhancing Aβ clearance.

## Discussion

In this study, we present a potential mechanism by which HCAA-associated mutations may drive cerebrovascular pathology, including CAA, fibrin(ogen) extravasation, altered BBB permeability, and AQP4 depolarization. Our results using siRNA-LNPs suggest that the aggravated CAA pathology in TgSwDI mice may be driven by two interrelated mechanisms. First, an age-dependent increase in Cav-1-mediated transcytosis facilitates fibrinogen extravasation into the perivascular space. The extravasated fibrin(ogen) binds to Aβ peptides, promoting fibrin(ogen) deposition, which further amplifies Cav-1 expression in a feedback loop that exacerbates the pathology. Simultaneously, fibrin(ogen)-Aβ co-deposits in the perivascular space activate microglia and may cause the depolarization of AQP4, further intensifying CAA formation. These findings underscore the complex interplay between Cav-1, fibrin(ogen) extravasation, and AQP4 delocalization, providing deeper insights into the progression of CAA.

In our study, we investigated the progression of CAA and associated pathology in TgSwDI mice at three age points: 7 months, 12 months, and 18 months, representing early, mid, and advanced phases of the disease, respectively. At 7 months, the mice exhibited the early phase, characterized by CAA development localized to the thalamus, but without detectable fibrinogen extravasation (SI Appendix Fig. S1) or significant changes in Cav-1 (SI Appendix Fig. S3) or AQP4 depolarization (SI Appendix Fig. S4). By 12 months, the mid-phase was marked by substantial fibrin(ogen) extravasation, increased CAA, and enhanced fibrin(ogen)-Aβ colocalization in both the hippocampus and thalamus (Fig. 1). This stage also showed elevated Cav-1 expression without significant changes in Mfsd2a expression (Fig. 2), along with AQP4 depolarization (Fig. 3). At 18 months, representing the advanced phase, the pathology had further intensified, with higher levels of fibrin(ogen) extravasation, an increased CAA burden, and more pronounced fibrin(ogen)-Aβ colocalization (Fig. 1). This stage also revealed a significant increase in Cav-1 levels, a reduction in Mfsd2a levels (Fig. 2), and continued loss of vascular AQP4 (Fig. 3). Our data suggest that the first pathological sign in TgSwDI mice is the deposition of vascular Aβ, which appears at 7 months of age, with the thalamus being the initial site of CAA

manifestation. At this early stage, there are no signs of fibrin(ogen) extravasation in any brain region, indicating that CAA precedes this aspect of vascular pathology.

Regulation of transcytosis is proposed as a critical mechanism for maintaining selective permeability of BBB in CNS (52, 65). Cav-1 mediated transcytosis plays an important role in compromising BBB integrity (50, 51). Brain tissues from AD patients show increased levels of Cav-1 in the hippocampus and frontal cortex, relative to age-matched control subjects (66). Our results showed significantly higher expression of endothelial Cav-1 in the hippocampus and thalamus of TgSwDI mice in an age dependent manner (Fig.2), suggesting that age may contribute to enhanced Cav-1 expression in these brain areas, as previously reported (67, 68). These brain regions also exhibit significant fibrin(ogen) extravasation at same ages (Fig. 1) indicating a temporal and spatial correlation between Cav-1 overexpression and the leakage of fibrin(ogen). Therefore, our results suggest that enhanced endothelial Cav-1 expression in TgSwDI mice may facilitate the leakage of fibrinogen into the perivascular area through non-specific caveolar transcytosis. Apart from our findings suggesting Cav-1's potential role in fibrinogen extravasation, there are reports suggesting that fibrinogen could also enhance endothelial Cav-1 levels. In a mice model of hyperfibrinogenemia, Muradashvili et al., demonstrated that elevated blood levels of fibrinogen alter cerebrovascular permeability mainly by increasing caveolae-mediated transcytosis (26) and elevating Cav-1 expression (27). As fibrin(ogen) binding to Aβ forms fibrinolysis resistant clot (19), once fibrinogen extravasates and binds to Aβ, it can persist in the perivascular space potentially leading to enhanced Cav-1 expression. Thus, our study demonstrating an age-dependent increase in Cav-1 levels in TgSwDI mice, along with a decrease in Cav-1 levels in siFga-treated TgSwDI mice, suggests that the accumulation of fibrin(ogen) in the perivascular space may also prompt endothelial cells to upregulate Cav-1 expression, in addition to the effects of aging itself. Furthermore, Caveolae-mediated transcytosis is negatively regulated by Mfsd2a, a lipid transporter expressed exclusively in brain endothelial cells. Mfsd2a transports omega-3 fatty acid docosahexaenoic acid (DHA) into the brain (52, 53, 69), displacing Cav-1 from the plasma membrane, which disrupts caveolae formation and inhibits caveolar transcytosis (70-72). We observed a significant decrease in Mfsd2a expression specifically in the hippocampus and thalamus of 18-months-old TgSwDI mice, but not in 12-months-old counterparts, when compared to WT littermates (Fig. 2). This reduction at advanced stages of CAA pathology may enhance caveolae function, potentially facilitating Cav-1-mediated fibrinogen transcytosis in the perivascular space, especially in older mice.

Our study showed a strong association between fibrin(ogen)-Aβ co-deposition and AQP4 depolarization. This finding is supported by several previous reports indicating the relationship between AQP4 and Aβ clearance, CAA pathology, and fibrinogen extravasation. *Aqp4* gene deletion and depolarization of AQP4, reduce Aβ clearance and promote microvascular Aβ deposition (31-35). Moreover, alterations in AQP4 expression and localization have been documented in AD and CAA patients across several reports (36-39). Fibrinogen extravasation is known to reduce perivascular AQP4 expression in iNPH patients, leading to the accumulation of brain metabolic waste and Aβ plaques, similar to what is observed in AD patients (42, 73). Additionally, our study demonstrated that CAA spread to the hippocampus as well as the thalamus, resulting in a progressive loss of perivascular AQP4 in both regions as TgSwDI mice aged to 12 and

18 months. CAA-laden vessels in both the hippocampus and thalamus exhibited significantly lower levels of perivascular AQP4 compared to CAA-free vessels (Fig. 3). Furthermore, fibrinogen depletion in siFga-treated TgSwDI mice decreased CAA and restored AQP4 depolarization in both brain regions. In summary, our study, along with previous findings, suggests a bidirectional relationship between CAA and AQP4 depolarization. Initially, CAA may induce AQP4 depolarization, contributing to impaired Aβ clearance and promoting the accumulation of amyloid plaques. As the disease progresses, the resulting AQP4 depolarization further exacerbates CAA pathology by diminishing perivascular AQP4 levels, creating a cycle that enhances both conditions. This interplay underscores the critical role of AQP4 in the pathophysiology of CAA and its potential impact on neurodegenerative processes.

Our findings indicated a central role of fibrin(ogen) in CAA pathology and thus we analyzed the beneficial effect of fibrin(ogen) knockdown in restoring normal physiology. Collectively, these results suggest that targeting fibrinogen may hold therapeutic promise for alleviating CAA-related pathology and improving cognitive dysfunction associated with AD. Studies of AD patient brains have shown an association between fibrinogen, Aβ and microglial reactivity in the perivascular region, which may contribute to neuronal damage (74). Activation of microglia in AD patients and mouse model is correlated with memory impairment (75-77). In multiple sclerosis, fibrinogen leakage upon BBB disruption induces rapid microglial responses around blood vessels (64). In an *in vivo* animal model of brain inflammation, induced by hippocampal injection of Aβ42 peptide, plasma fibrinogen depletion with ancrod significantly reduced vascular microgliosis but not astrogliosis (74). In our study, we observed a reduction in microglial activation within CAA-affected areas in fibrinogen-depleted TgSwDI mice compared to those with normal fibrinogen levels (Fig. 5). However, no significant changes in GFAP immunoreactivity between fibrinogen-depleted TgSwDI and those with normal blood fibrinogen levels, suggesting that fibrinogen depletion does not significantly affect reactive astrocyte populations in TgSwDI mice (SI Appendix Fig. S6A and B).

Our study elucidates the mechanisms by which HCAA-linked APP mutations lead to cerebrovascular dysfunctions, highlighting the critical role of fibrin(ogen) in CAA pathology. We propose that the age-dependent increase in Cav-1 expression in TgSwDI mice may contribute to fibrin(ogen) extravasation. This extravasation allows fibrinogen to bind to Aβ, triggering microglial neuroinflammation and AQP4 depolarization, which worsens CAA pathology. Fibrin(ogen) knockdown not only reduced CAA pathology but also improved cognitive function, suggesting the therapeutic potential of targeting fibrin(ogen) in CAA-related pathologies, including AD.

## Materials and Methods

### *Animals.*

TgSwDI (The Jackson Laboratory, stock #034843-JAX) are transgenic mice on C57BL/6 background that express human APP gene (isoform 770) containing the Swedish (K670N/M671L), Dutch (E693Q), and Iowa (D694N) mutations under the control of the mouse Thy1 promoter (78). The Swedish K670N/M671L mutation results in enhance β-

secretase processing and increased production of Aβ. Dutch and Iowa mutations increase CAA in the brain of TgSwDI mice (78). TgSwDI hemizygous transgenic mice and WT littermate controls were used in the entire study. The mice were housed under a 12-hour light/dark cycle and had ad libitum access to food and water. All work involving the maintenance, breeding, and experimentation with animals adhered to protocols approved by the Rutgers University Institutional Animal Care and Use Committee.

*Intravenous administration of siRNA lipid nano particles.*

A previously identified 2'*O*-methylated siRNA sequence targeting murine fibrinogen (*Fga)* mRNA was used (56) and an siRNA targeting luciferase (siLuc) was applied as a negative control. Sequences were obtained commercially by Integrated DNA Therapeutics (IDT) and siRNAs were encapsulated in lipid nanoparticle (LNP) as previously described (79). Briefly, siRNAs were dissolved in sodium acetate (pH 4) and combined with a lipid solution at an amine-to-phosphate (N/P) ratio of 3. The LNP consisted of an ionizable cationic lipid, DLin-MC3-DMA, and 3 helper lipids: cholesterol, DSPC and PEG-DMG at a 50: 38.5:10:1.5 % molar ratio (Avanti Lipids). The LNP were dialyzed against Dulbecco's phosphate buffered saline (PBS) at pH 7.4 in 500-fold volume excess. Cholesterol content was measured using the Cholesterol E Assay Kit (Wako Chemicals, Mountain View, CA USA) and RiboGreen assay (Quant-IT Ribogreen RNA Assay Kit, ThermoFisher) was performed to determine mRNA concentration and encapsulation efficiency. siRNA-LNP were diluted to 0.2 mg/mL with a buffer containing 10 mM L-histidine and 10% sucrose (pH 7.4) and stored at −80°C. 9 months-old TgSwDI mice and WT littermates were intravenously injected with LNP-encapsulated siRNA targeting the fibrinogen alpha chain (siFga) and siRNA sequence targeting luciferase (siLuc) as a negative control, every 10 days for three months.

## Immunohistochemistry

TgSwDI mice at age of 7- or 12- or 18 months, or mice administered with siRNA-LNPs were perfused transcardially with 0.9% saline plus 2.5% heparin solution, followed by extraction of brains and embedding them in optical cutting temperature (OCT) medium. Brains were frozen and then sectioned (20μm) coronally, using cryostat (Leica CM1950). Sections were mounted on glass slides and immunohistochemistry was performed. Sections were fixed with chilled methanol: acetone (1:1) for 5 minutes or 4 % paraformaldehyde for 20 minutes at room temperature. Sections were then washed with PBS and then blocked in PBST (PBS+0.3% Tritonx-100) with 5% normal donkey serum for 1 hour at room temperature in humidified chamber. Thereafter, sections were incubated with primary antibody overnight diluted in PBST solution (PBS+0.1% TritonX-100) with 5% normal donkey serum at 4ºC in humidified chamber. The primary antibody used were 1) Anti-amyloid-beta, 1-16 (6E10) conjugated to Alexa Fluor 488 (1/250) (BioLegend, 803013), 2) anti-fibrinogen (1/500) (Dako, A008002-2), 3) anti-collagen IV (1/250) (Millipore, AB769), 4) anti-Caveolin-1 (1/1000) (Cell signalling technology, 3267S), 5) anti- Mfsd2a (1/200) (Cell signalling technology, 80302), 6) anti-CD31 (1/30) (BD Pharmingen, 550274), 7) anti- CD11b (1/200) (Cell signalling technology, 17800), 8) anti-GFAP (1/250) (Thermofisher scientific, 3-0300), 9) anti-AQP4 (1/500) (Cell signalling technology, 59678S). Sections were then washed 3 times with PBST (PBS+0.05% TritonX-100) for 5 minutes on shaker. Thereafter, sections were incubated with secondary antibodies, diluted in PBST (PBS+0.1% TritonX-100) with 5 % donkey

serum for 1 hour at room temperature in humidified chamber. The secondary antibodies were tagged with Alexa Flour 405 or 488 or 555 or 647 fluorophores. The sections were washed 3 times with PBST (PBS+0.05% TritonX-100) for 5 minutes on shaker. The sections were incubated with Sudan black b (Sigma, 199664) for 1 minute to diminish lipofuscin autofluorescence and then washed with 70% ethanol for 20 seconds, followed by washing with PBS, 3 times for 5 minutes on shaker. The sections were then mounted with Vectashield® antifade mounting medium (Vectorlabs, H-1000-10) and cover slipped. For fibrin(ogen)-Aβ co-deposition imaging, Nikon A1R confocal microscope was used, while other images were acquired using Nikon eclipse Ti2 fluorescence microscope and NIS elements AR software. The images were analyzed using Fiji-ImageJ software. Perivascular and total CD11b area was quantified in siRNA LNP's treated mice using MatLab Image Processing Toolbox tool. CD11b signals were taken as vascular, if 10% or more colocalize with Collagen IV signals. To assess this, we created a MatLab code (Supplementary File 1) which determines boundary boxes around continuous objects in the CD11b staining channel that were larger than 20 square microns. For each continuous object selected, we calculated the area of CD11b staining as well as area of collagen IV staining. Using these two parameters, we were able to determine which areas of CD11b fell into the category of vascular CD11b staining. MATLAB was employed in this analysis to provide consistent and unbiased tools for separating and quantifying vascular CD11b staining from nonvascular CD11b staining.

## Prussian blue staining

We used iron stain kit (abcam, ab150674) which detects ferric iron in tissues, formed after the lysis of RBCs. Ferric iron reacts with acid ferrocyanide producing a blue color (Prussian Blue stain reaction) (45). Prussian blue iron staining was performed as described previously (80, 81). Briefly, tissue sections from 18-months-old TgSwDI mice and WT littermates were fixed in 4% PFA in PBS for 20 minutes at RT. The sections were then incubated for 3 minutes in iron stain, which is a 1:1 mixture of potassium ferrocyanide and hydrochloric acid. The tissues were washed thoroughly with distilled water, followed by counterstaining with nuclear fast red solution for 5 minutes. The sections were then washed again 4 times with distilled water, 5 minutes each and then dehydrated in 95% ethanol followed by absolute alcohol. The sections were then mounted with VectaMount™ Mounting Medium (Vectorlabs, H-5000) followed by visualization under the brightfield microscope.

## Evans blue assay

Blood brain barrier integrity was observed using Evans blue dye as described previously with slight modification (82). A 2% solution of Evans Blue dye in normal saline was injected intraperitoneally in 18-months-old TgSwDI and WT littermates (10ul dye/g of body weight). The dye was allowed to circulate for 6 hours. Afterwards, the mice were transcardially perfused with 30ml of ice-cold saline, plus 2.5% heparin solution and the brain tissue were removed, weighed, homogenized in 50% TCA in 1:3 weight to volume ratio and incubated for 1 hour on ice. Samples were centrifuged for 30 minutes at 10000g at 4º C. 30ul of supernatant and 90ul of 95% ethanol was added in single well of 96 well plate. Each sample was in triplicate. Evans Blue dye content in brain tissue was

measured by reading absorbance at 620 nm and quantified according to a standard curve. The results are presented as ng of Evans Blue stain/mg of tissue.

## Barnes Maze Test

Spatial memory was measured using a Barnes maze as previously described (62) with slight modifications. The test was performed on 12 months-old siRNA- LNP treated mice. Testing room contained stationary visual cues, and the tester remained in a specific position during testing. The maze consisted of a white circular platform 92 cm in diameter with 20 holes (5.5 cm diameter) evenly spaced around the perimeter. One hole was assigned as a target for each mouse and led to a small dark target hole (escape box). All other holes had false bottoms. For motivation, the maze was illuminated with two halogen lamps in addition to room lighting producing an illumination of 1200 lux at the maze surface. The mice were kept in the center of the platform and trained to locate target hole within 300 seconds. If the mouse failed to find the target hole within 300 seconds, it was then gently guided to the box and allowed to remain in the target hole for 30 seconds before being returned to its home cage. If the mouse found the target hole, it was immediately returned to its home cage. The mice underwent two trials per day for three consecutive days using the same training method. Following this, probe trials were conducted 24 hours after the final training session. During the probe trials, all the holes were closed, and the mice were allowed to explore for 120 seconds. The mouse's movements were monitored with a camera interfaced to a computer which operated video tracking software (Noldus, EthoVision XT 14). An examination of the latency to find the target hole and cumulative duration in target hole was analyzed.

## Western blot Assay

Brain tissue form 18-months-old TgSwDI mice and WT littermates, and 12-months-old siRNA treated TgSwDI mice and WT littermates were lysed in radioimmunoprecipitation assay (RIPA) buffer (25 mM Tris•HCl pH 7.6, 150 mM NaCl, 1% NP-40, 1% sodium deoxycholate, 0.1% SDS (Thermofisher scientific, #89900) along with protease and phosphatase inhibitor cocktail (Thermofisher #A32962) and centrifugated for 15 min at 10,000 rpm, 4ºC. Tissue lysates were quantified using the BCA protein assay (Pierce #23223) and samples for western blot was prepared. 30 µg of protein was loaded per well on Bolt™ Bis-Tris Plus Mini Protein Gels, 4-12% (Thermofisher scientific, #NW04125BOX) with Bolt MES SDS Running Buffer (Invitrogen, #B0002). Gels were transferred onto Immobilon®-P PVDF Membrane (Millipore sigma, #IPVH85R) using Tris transfer buffer [400 mmol/mL Tris base, 70 mmol/mL glycine, 10% methanol]. Membrane was blocked in 5% milk in TBST (Tris Buffer salin+0.1% Tween-20) at RT for 1 hour on orbital shaker. Thereafter, membranes were incubated with primary antibodies diluted in 5% milk TBST (Tris Buffer salin+0.1% Tween-20) overnight at 4ºC on shaker. Primary antibodies used were rabbit anti-ZO-1 (1:1000, Invitrogen #40-2200), rabbit anti-Claudin-5 (1/1000, Invitrogen # 341600), rabbit anti-Occludin (1/1000 Abcam # ab167161), rabbit anti-fibrinogen (1/5000, Dako, A008002), mouse anti GAPDH (1/10000, Abcam, ab9484) and rabbit anti-transferrin (1/1000, Cell signalling # 35293). Next, membranes were washed with TBST (Tris Buffer salin+0.1% Tween-20), 3 times for 10 minutes each. Then, membranes were incubated with secondary antibodies: donkey anti rabbit IgG conjugated to horseradish peroxidase (HRP) (1/20000, Cytiva, NA934V) and sheep anti mouse IgG conjugated to HRP (Cytiva, NA931V) diluted in 5% milk TBST for 1 hour at

RT on shaker. Membranes were then washed with TBST, 10 minutes on shaker and developed by using Pierce™ ECL Plus Western Blotting Substrate (Thermo fisher #32134). PVDF membranes were imaged using iBright™ CL1500 Imaging System and analyzed by densitometry using Fiji-Image J software. Data was expressed in arbitrary densitometry units (ADU).

## Statistical analysis

Bar graphs were created using GraphPad Prism 8 (GraphPad Software, San Diego, CA). Statistical analyses were conducted using Prism 8. All numerical values presented in graphs are mean ± SEM. Statistical analyses were assessed as described in the text using either one-way or two-way ANOVA followed by Bonferroni multiple comparisons post-hoc analysis or two-tailed unpaired t test. P values below 0.05 were considered significant. P values were as follows: ***$P < 0.001$; **$P < 0.01$; *$P < 0.05$.

## Acknowledgments

This work was supported by NIH Grants NS104386 (to H.J.A.), and AG078245 (to H.J.A.). We thank the Cellular Imaging and Histology Core, Rutgers, Newark for assistance with confocal microscopy. We also thank Kelly Mulraney, veterinary staff at In Vivo Research Services (IVRS) core, Rutgers, for assisting with tail vein injections of siRNA LNP's. We thank members of the Ahn laboratory for scientific discussion, and experimental support.

## References


1. C. C. Hays, Z. Z. Zlatar, C. E. Wierenga, The Utility of Cerebral Blood Flow as a Biomarker of Preclinical Alzheimer's Disease. Cell Mol Neurobiol 36, 167-179 (2016).

2. M. A. Binnewijzend et al., Cerebral perfusion in the predementia stages of Alzheimer's disease. Eur Radiol 26, 506-514 (2016).

3. R. D. Bell, B. V. Zlokovic, Neurovascular mechanisms and blood-brain barrier disorder in Alzheimer's disease. Acta Neuropathol 118, 103-113 (2009).

4. N. A. Johnson et al., Pattern of cerebral hypoperfusion in Alzheimer disease and mild cognitive impairment measured with arterial spin-labeling MR imaging: initial experience. Radiology 234, 851-859 (2005).

5. A. Serrano-Pozo et al., Examination of the clinicopathologic continuum of Alzheimer disease in the autopsy cohort of the National Alzheimer Coordinating Center. J Neuropathol Exp Neurol 72, 1182-1192 (2013).

6. M. Yamada, Cerebral amyloid angiopathy: emerging concepts. J Stroke 17, 17-30 (2015).

7. D. R. Thal et al., Capillary cerebral amyloid angiopathy is associated with vessel occlusion and cerebral blood flow disturbances. Neurobiol Aging 30, 1936-1948 (2009).

8. E. E. Smith et al., Impaired visual evoked flow velocity response in cerebral amyloid angiopathy. Neurology 71, 1424-1430 (2008).

9. J. P. Vonsattel et al., Cerebral amyloid angiopathy without and with cerebral hemorrhages: a comparative histological study. Ann Neurol 30, 637-649 (1991).

10. A. Lauer et al., Microbleeds on MRI are associated with microinfarcts on autopsy in cerebral amyloid angiopathy. Neurology 87, 1488-1492 (2016).

11. A. Viswanathan, S. M. Greenberg, Cerebral amyloid angiopathy in the elderly. Ann Neurol 70, 871-880 (2011).

12. A. Biffi, Main features of hereditary cerebral amyloid angiopathies: A systematic review. Cereb Circ Cogn Behav 3, 100124 (2022).

13. A. Biffi, S. M. Greenberg, Cerebral amyloid angiopathy: a systematic review. J Clin Neurol 7, 1-9 (2011).

14. K. Rannikmae, N. Samarasekera, N. A. Martinez-Gonzalez, R. Al-Shahi Salman, C. L. Sudlow, Genetics of cerebral amyloid angiopathy: systematic review and meta-analysis. J Neurol Neurosurg Psychiatry 84, 901-908 (2013).

15. T. Revesz et al., Sporadic and familial cerebral amyloid angiopathies. Brain Pathol 12, 343-357 (2002).

16. S. X. Zhang-Nunes et al., The cerebral beta-amyloid angiopathies: hereditary and sporadic. Brain Pathol 16, 30-39 (2006).

17. P. Fotiadis et al., Cortical atrophy in patients with cerebral amyloid angiopathy: a case-control study. Lancet Neurol 15, 811-819 (2016).

18. S. A. Cajamarca, E. H. Norris, L. van der Weerd, S. Strickland, H. J. Ahn, Cerebral amyloid angiopathy-linked beta-amyloid mutations promote cerebral fibrin deposits via increased binding affinity for fibrinogen. Proc Natl Acad Sci U S A 117, 14482-14492 (2020).

19. H. J. Ahn, S. K. Baker, E. H. Norris, S. Strickland, Inflaming the Brain. Neuron 101, 991-993 (2019).

20. J. Paul, S. Strickland, J. P. Melchor, Fibrin deposition accelerates neurovascular damage and neuroinflammation in mouse models of Alzheimer's disease. J Exp Med 204, 1999-2008 (2007).

21. M. Cortes-Canteli, L. Mattei, A. T. Richards, E. H. Norris, S. Strickland, Fibrin deposited in the Alzheimer's disease brain promotes neuronal degeneration. Neurobiol Aging 36, 608-617 (2015).

22. H. E. Berk-Rauch et al., Striatal fibrinogen extravasation and vascular degeneration correlate with motor dysfunction in an aging mouse model of Alzheimer's disease. Front Aging Neurosci 15, 1064178 (2023).

23. N. M. Tataryn et al., Vascular endothelial growth factor associated dissimilar cerebrovascular phenotypes in two different mouse models of Alzheimer's Disease. Neurobiol Aging 107, 96-108 (2021).

24. A. C. Yang et al., Physiological blood-brain transport is impaired with age by a shift in transcytosis. Nature 583, 425-430 (2020).

25. P. G. Frank, S. Pavlides, M. P. Lisanti, Caveolae and transcytosis in endothelial cells: role in atherosclerosis. Cell Tissue Res 335, 41-47 (2009).

26. N. Muradashvili, R. Tyagi, N. Tyagi, S. C. Tyagi, D. Lominadze, Cerebrovascular disorders caused by hyperfibrinogenaemia. J Physiol 594, 5941-5957 (2016).

27. N. Muradashvili, R. L. Benton, R. Tyagi, S. C. Tyagi, D. Lominadze, Elevated level of fibrinogen increases caveolae formation; role of matrix metalloproteinase-9. Cell Biochem Biophys 69, 283-294 (2014).

28. R. E. Day et al., Human aquaporins: regulators of transcellular water flow. Biochim Biophys Acta 1840, 1492-1506 (2014).

29. M. C. Papadopoulos, A. S. Verkman, Aquaporin water channels in the nervous system. Nat Rev Neurosci 14, 265-277 (2013).

30. S. Mader, L. Brimberg, Aquaporin-4 Water Channel in the Brain and Its Implication for Health and Disease. Cells 8 (2019).

31. N. J. Abbott, M. E. Pizzo, J. E. Preston, D. Janigro, R. G. Thorne, The role of brain barriers in fluid movement in the CNS: is there a 'glymphatic' system? Acta Neuropathol 135, 387-407 (2018).

32. M. K. Rasmussen, H. Mestre, M. Nedergaard, The glymphatic pathway in neurological disorders. Lancet Neurol 17, 1016-1024 (2018).

33. J. J. Iliff et al., Impairment of glymphatic pathway function promotes tau pathology after traumatic brain injury. J Neurosci 34, 16180-16193 (2014).

34. K. Ishida et al., Glymphatic system clears extracellular tau and protects from tau aggregation and neurodegeneration. J Exp Med 219 (2022).

35. T. J. Pedersen, S. A. Keil, W. Han, M. X. Wang, J. J. Iliff, The effect of aquaporin-4 mis-localization on Abeta deposition in mice. Neurobiol Dis 181, 106100 (2023).

36. P. Marazuela et al., Circulating AQP4 Levels in Patients with Cerebral Amyloid Angiopathy-Associated Intracerebral Hemorrhage. J Clin Med 10 (2021).

37. Y. L. Lan, J. Zhao, T. Ma, S. Li, The Potential Roles of Aquaporin 4 in Alzheimer's Disease. Mol Neurobiol 53, 5300-5309 (2016).

38. C. Yang et al., Aquaporin-4 and Alzheimer's Disease. J Alzheimers Dis 52, 391-402 (2016).

39. D. M. Wilcock, M. P. Vitek, C. A. Colton, Vascular amyloid alters astrocytic water and potassium channels in mouse models and humans with Alzheimer's disease. Neuroscience 159, 1055-1069 (2009).

40. M. Simon et al., Loss of perivascular aquaporin-4 localization impairs glymphatic exchange and promotes amyloid beta plaque formation in mice. Alzheimers Res Ther 14, 59 (2022).

41. J. J. Iliff et al., A paravascular pathway facilitates CSF flow through the brain parenchyma and the clearance of interstitial solutes, including amyloid beta. Sci Transl Med 4, 147ra111 (2012).

42. P. K. Eide, H. A. Hansson, Blood-brain barrier leakage of blood proteins in idiopathic normal pressure hydrocephalus. Brain Res 1727, 146547 (2020).

43. Y. Shin, H. S. Cho, G. W. Rebeck, S. M. Greenberg, Vascular changes in Iowa-type hereditary cerebral amyloid angiopathy. Ann N Y Acad Sci 977, 245-251 (2002).

44. M. Maat-Schieman, R. Roos, S. van Duinen, Hereditary cerebral hemorrhage with amyloidosis-Dutch type. Neuropathology 25, 288-297 (2005).

45. S. Liu et al., Comparative analysis of H&E and Prussian blue staining in a mouse model of cerebral microbleeds. J Histochem Cytochem 62, 767-773 (2014).

46. Y. Okamoto et al., Cerebral hypoperfusion accelerates cerebral amyloid angiopathy and promotes cortical microinfarcts. Acta Neuropathol 123, 381-394 (2012).

47. S. Saito et al., Taxifolin inhibits amyloid-beta oligomer formation and fully restores vascular integrity and memory in cerebral amyloid angiopathy. Acta Neuropathol Commun 5, 26 (2017).

48. M. Wolman et al., Evaluation of the dye-protein tracers in pathophysiology of the blood-brain barrier. Acta Neuropathol 54, 55-61 (1981).

49. H. L. Wang, T. W. Lai, Optimization of Evans blue quantitation in limited rat tissue samples. Sci Rep 4, 6588 (2014).

50. P. C. Nahirney, P. Reeson, C. E. Brown, Ultrastructural analysis of blood-brain barrier breakdown in the peri-infarct zone in young adult and aged mice. J Cereb Blood Flow Metab 36, 413-425 (2016).

51. M. J. Haley, C. B. Lawrence, The blood-brain barrier after stroke: Structural studies and the role of transcytotic vesicles. J Cereb Blood Flow Metab 37, 456-470 (2017).

52. B. J. Andreone et al., Blood-Brain Barrier Permeability Is Regulated by Lipid Transport-Dependent Suppression of Caveolae-Mediated Transcytosis. Neuron 94, 581-594 e585 (2017).

53. M. Zhou et al., Caveolae-Mediated Endothelial Transcytosis across the Blood-Brain Barrier in Acute Ischemic Stroke. J Clin Med 10 (2021).

54. M. Cortes-Canteli et al., Fibrinogen and beta-amyloid association alters thrombosis and fibrinolysis: a possible contributing factor to Alzheimer's disease. Neuron 66, 695-709 (2010).

55. D. E. Levy et al., Ancrod in acute ischemic stroke: results of 500 subjects beginning treatment within 6 hours of stroke onset in the ancrod stroke program. Stroke 40, 3796-3803 (2009).

56. L. J. Juang et al., Suppression of fibrin(ogen)-driven pathologies in disease models through controlled knockdown by lipid nanoparticle delivery of siRNA. Blood 139, 1302-1311 (2022).

57. G. E. Hernandez et al., Aortic intimal resident macrophages are essential for maintenance of the non-thrombogenic intravascular state. Nat Cardiovasc Res 1, 67-84 (2022).

58. W. S. Hur et al., Elimination of fibrin polymer formation or crosslinking, but not fibrinogen deficiency, is protective against diet-induced obesity and associated pathologies. J Thromb Haemost 20, 2873-2886 (2022).

59. W. S. Hur et al., Hypofibrinogenemia with preserved hemostasis and protection from thrombosis in mice with an Fga truncation mutation. Blood 139, 1374-1388 (2022).

60. F. Xu et al., Early-onset subicular microvascular amyloid and neuroinflammation correlate with behavioral deficits in vasculotropic mutant amyloid beta-protein precursor transgenic mice. Neuroscience 146, 98-107 (2007).

61. L. S. Robison et al., Long-term voluntary wheel running does not alter vascular amyloid burden but reduces neuroinflammation in the Tg-SwDI mouse model of cerebral amyloid angiopathy. J Neuroinflammation 16, 144 (2019).

62. S. E. Setti, T. Flanigan, J. Hanig, S. Sarkar, Assessment of sex-related neuropathology and cognitive deficits in the Tg-SwDI mouse model of Alzheimer's disease. Behav Brain Res 428, 113882 (2022).

63. S. Rotshenker, Microglia and macrophage activation and the regulation of complement-receptor-3 (CR3/MAC-1)-mediated myelin phagocytosis in injury and disease. J Mol Neurosci 21, 65-72 (2003).

64. D. Davalos et al., Fibrinogen-induced perivascular microglial clustering is required for the development of axonal damage in neuroinflammation. Nat Commun 3, 1227 (2012).

65. B. W. Chow, C. Gu, Gradual Suppression of Transcytosis Governs Functional Blood-Retinal Barrier Formation. Neuron 93, 1325-1333 e1323 (2017).

66. S. B. Gaudreault, D. Dea, J. Poirier, Increased caveolin-1 expression in Alzheimer's disease brain. Neurobiol Aging 25, 753-759 (2004).

67. T. Y. Ha et al., Age-related increase in caveolin-1 expression facilitates cell-to-cell transmission of alpha-synuclein in neurons. Mol Brain 14, 122 (2021).

68. M. J. Kang et al., Caveolin-1 upregulation in senescent neurons alters amyloid precursor protein processing. Exp Mol Med 38, 126-133 (2006).

69. A. Ben-Zvi et al., Mfsd2a is critical for the formation and function of the blood-brain barrier. Nature 509, 507-511 (2014).

70. W. Chen, D. B. Jump, W. J. Esselman, J. V. Busik, Inhibition of cytokine signaling in human retinal endothelial cells through modification of caveolae/lipid rafts by docosahexaenoic acid. Invest Ophthalmol Vis Sci 48, 18-26 (2007).

71. Q. Li et al., Docosahexaenoic acid affects endothelial nitric oxide synthase in caveolae. Arch Biochem Biophys 466, 250-259 (2007).

72. D. W. Ma et al., n-3 PUFA alter caveolae lipid composition and resident protein localization in mouse colon. FASEB J 18, 1040-1042 (2004).

73. B. C. Reeves et al., Glymphatic System Impairment in Alzheimer's Disease and Idiopathic Normal Pressure Hydrocephalus. Trends Mol Med 26, 285-295 (2020).

74. J. K. Ryu, J. G. McLarnon, A leaky blood-brain barrier, fibrinogen infiltration and microglial reactivity in inflamed Alzheimer's disease brain. J Cell Mol Med 13, 2911-2925 (2009).

75. T. A. Bayer, R. Buslei, L. Havas, P. Falkai, Evidence for activation of microglia in patients with psychiatric illnesses. Neurosci Lett 271, 126-128 (1999).

76. G. Dhawan, C. K. Combs, Inhibition of Src kinase activity attenuates amyloid associated microgliosis in a murine model of Alzheimer's disease. J Neuroinflammation 9, 117 (2012).

77. J. Vom Berg et al., Inhibition of IL-12/IL-23 signaling reduces Alzheimer's disease-like pathology and cognitive decline. Nat Med 18, 1812-1819 (2012).

78. J. Davis et al., Early-onset and robust cerebral microvascular accumulation of amyloid beta-protein in transgenic mice expressing low levels of a vasculotropic Dutch/Iowa mutant form of amyloid beta-protein precursor. J Biol Chem 279, 20296-20306 (2004).

79. F. Ferraresso et al., Comparison of DLin-MC3-DMA and ALC-0315 for siRNA Delivery to Hepatocytes and Hepatic Stellate Cells. Mol Pharm 19, 2175-2182 (2022).

80. G. Gomori, Microtechnical Demonstration of Iron: A Criticism of its Methods. Am J Pathol 12, 655-664 651 (1936).

81. D. T. Winkler et al., Spontaneous hemorrhagic stroke in a mouse model of cerebral amyloid angiopathy. J Neurosci 21, 1619-1627 (2001).

82. A. Manaenko, H. Chen, J. Kammer, J. H. Zhang, J. Tang, Comparison Evans Blue injection routes: Intravenous versus intraperitoneal, for measurement of blood-brain barrier in a mice hemorrhage model. J Neurosci Methods 195, 206-210 (2011).

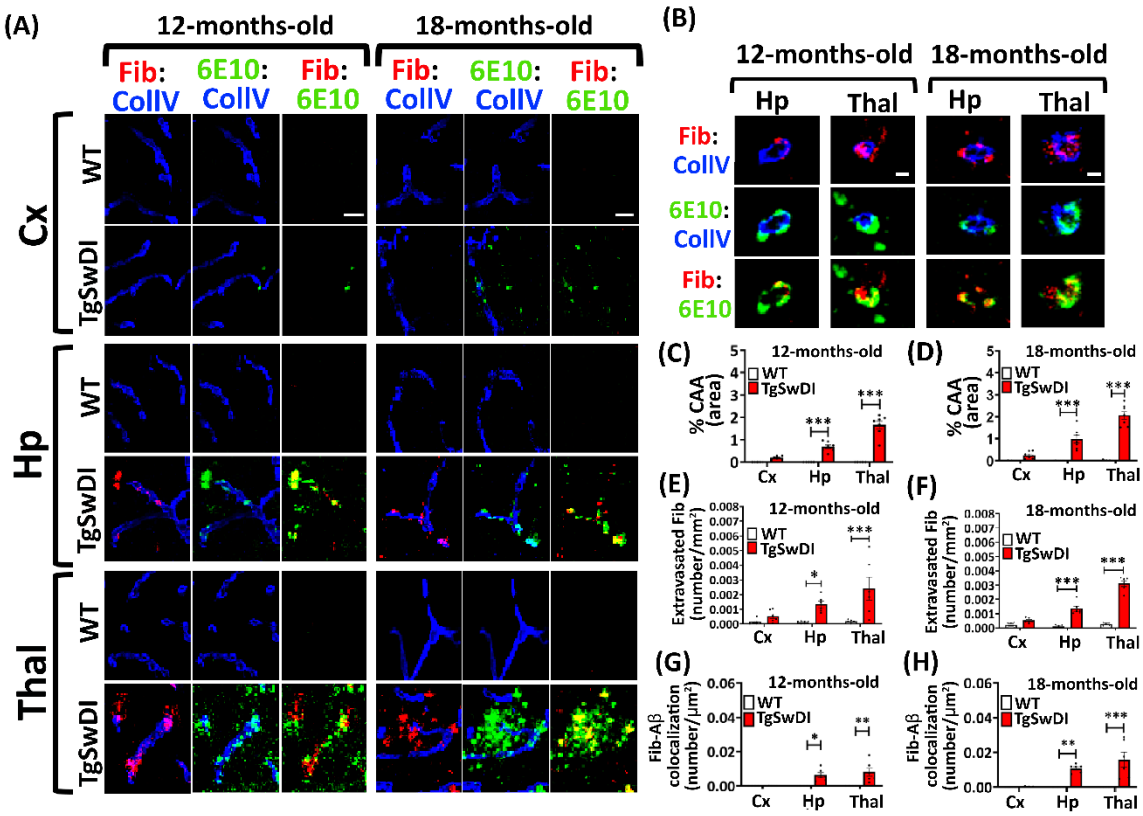


**Figure 1.** The age-dependent increase of fibrin(ogen) extravasation, CAA and Aβ-fibrin(ogen) co-deposition in the brain of TgSwDI mice. (A) Representative images of brain coronal sections were probed with antibodies against fibrin(ogen) (Fib, red), Aβ (6E10, green), and blood vessels (collagen IV (CollV), blue). CAA is represented as colocalized collagen IV and Aβ. Significant increased extravasation of fibrin(ogen), CAA and fibrin(ogen)-Aβ colocalization in hippocampus and thalamus of 12- and 18-months-old TgSwDI compared to WT littermates (12-months-old mice, n=6 per group; 18-months-old mice, n=5-6 per group). Scale bar= 20μm. (B) Images of single blood vessel view showed Aβ-fibrin(ogen) co-deposition in perivascular region of 12- and 18-months-old TgSwDI. Scale bar= 5μm. Quantification of % CAA in 12-months (C) and 18-months-old (D) TgSwDI mice and WT littermates and number of extravasated fibrin(ogen) spots in 12-months (E) and 18-months-old (F) TgSwDI mice and WT littermates. Quantification of significant increase of fibrin(ogen)-Aβ colocalization in TgSwDI mice compared to WT littermates at both 12- (G) and18-months of age (H). Data were analyzed by using two-way ANOVA with the Bonferroni post hoc test and shown as average ± SEM; *, $P < 0.05$, **, $P < 0.01$, ***$P < 0.001$. Fib=Fibrin(ogen), CollV=Collagen IV, Cx=Cortex, Hp=Hippocampus, Thal=Thalamus.

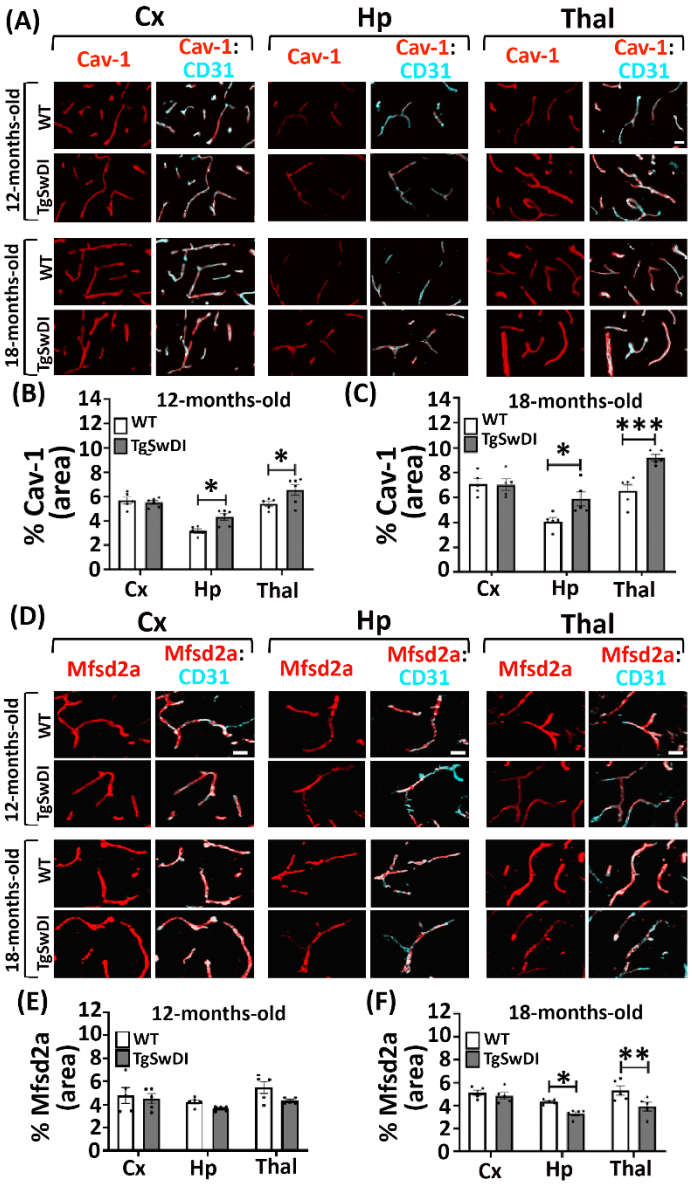


**Figure 2**. The age dependent altered expression of Cav-1 and Mfsd2a in the brain of TgSwDI mice. (A) Representative images of brain coronal sections were probed with antibodies against Cav-1 (red) and endothelial cell marker- CD31 (cyan). (B, C) Quantification of Cav-1 showed significant increase of Cav-1 in hippocampus and thalamus of 12- and 18-months-old TgSwDI compared to WT littermates (12-months-old mice, n=5-6 per group; 18-months-old mice, n=5 per group). Scale bar= 20µm. (D) IHC images showing significant decrease of Mfsd2a (red) in hippocampus and thalamus of 12- and18-months-old TgSwDI compared to WT littermates (12-months-old mice, n=5 per group; 18-months-old mice n=5 per group). Scale bar= 20µm. (E, F) Quantification of Mfsd2a, as represented in (D). Data were analyzed by using two-way ANOVA with the Bonferroni post hoc test and shown as average ± SEM; *, $P < 0.05$, **, $P < 0.01$, ***$P < 0.001$.

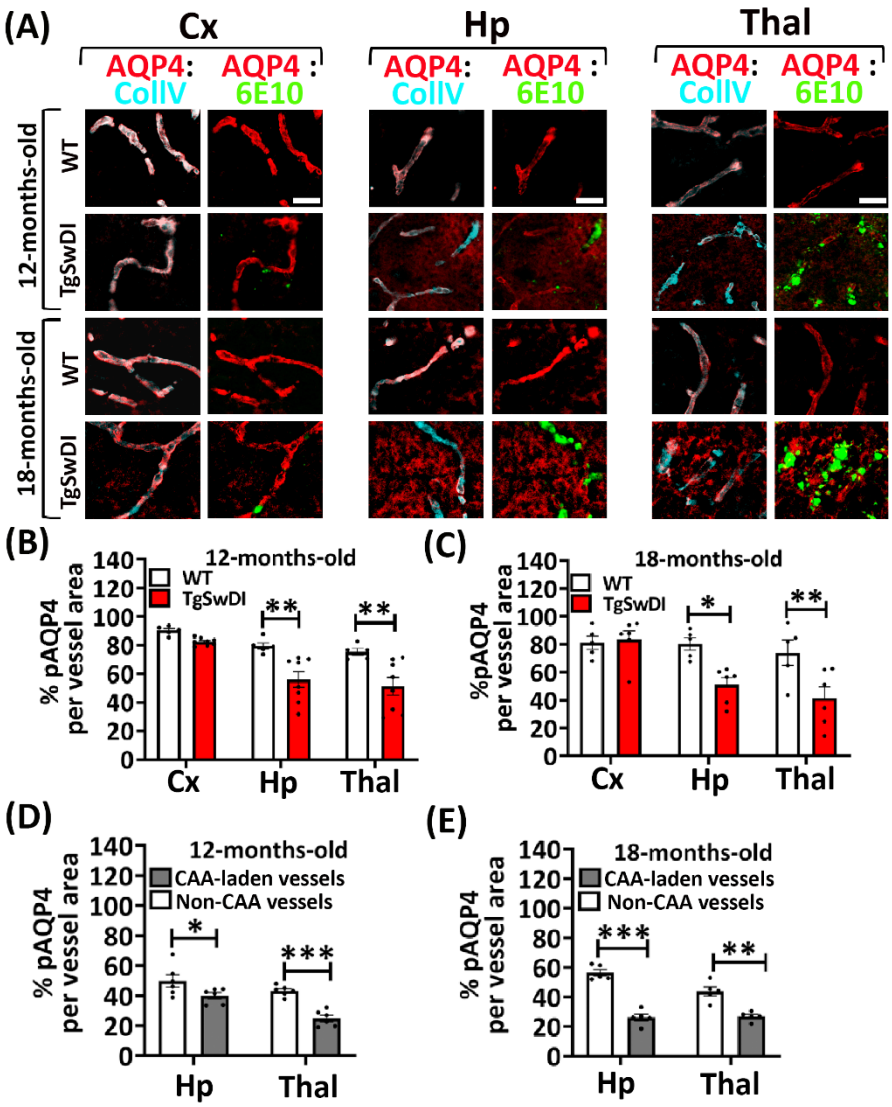


**Figure 3**. The age dependent decrease of perivascular AQP4 in the brain of TgSwDI mice. (A) Representative images of brain coronal sections were probed with antibodies against AQP4 (red), Aβ (6E10, green), and blood vessels (collagen IV, cyan). Perivascular AQP4 is pink in color. Scale bar= 20μm. (B – C) Quantification of perivascular AQP4 of 12- and 18-months-old TgSwDI compared to WT littermates. (12-months-old mice, n=5-8 per group; 18-months-old mice, n=5 per group). A significant loss of perivascular AQP4 in the hippocampus and thalamus of 12- and 18-months-old TgSwDI mice. (D- E) Quantification of perivascular AQP4 in CAA-laden vessels compared to non-CAA vessels in 12- and 18-months-old TgSwDI. Perivascular AQP4 in CAA-laden vessels decreased significantly in hippocampus and thalamus, compared to non-CAA vessels in 12- and 18-months-old TgSwDI mice. Data were analyzed by using two-way ANOVA with the Bonferroni post hoc test and shown as average ± SEM; *, $P < 0.05$, **, $P < 0.01$, ***$P < 0.001$. pAQP4=Perivascular AQP4.

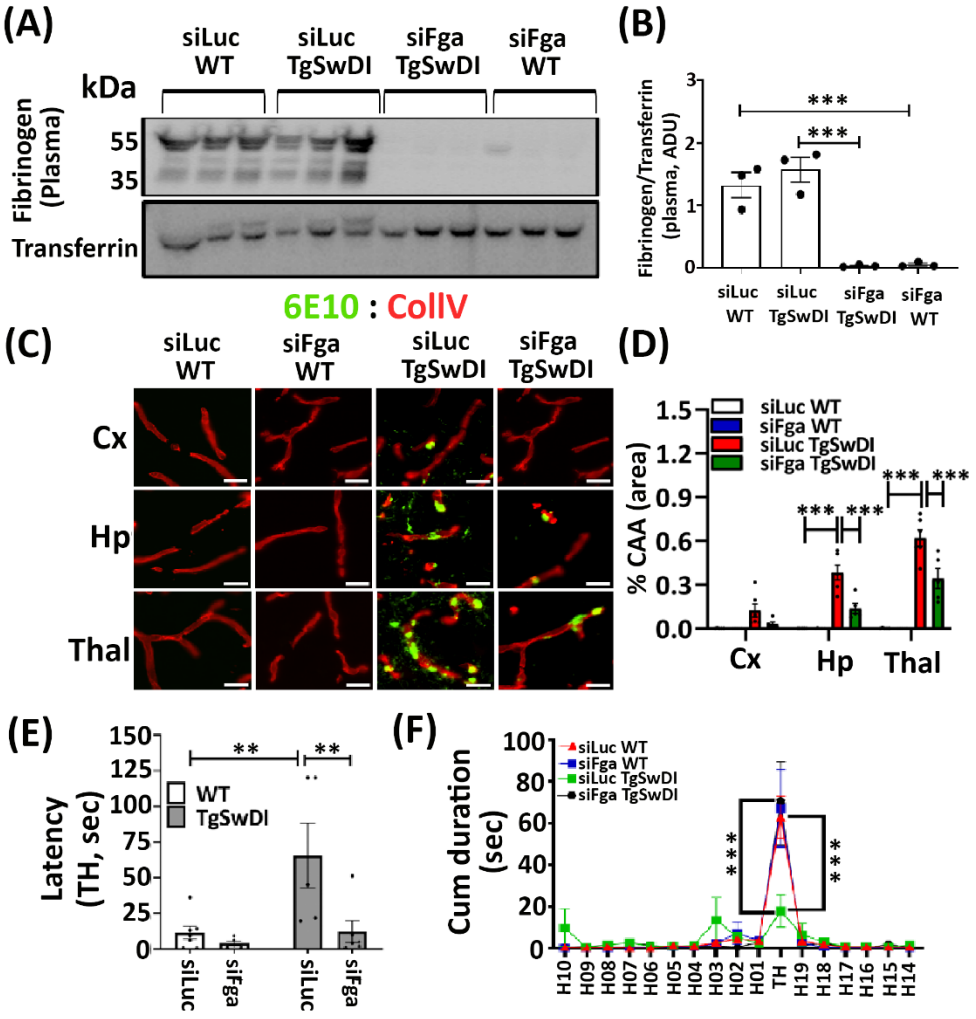


**Figure 4.** Depletion of fibrinogen significantly reducing CAA and restoring spatial memory in TgSwDI mice. (A) Western blot analysis confirming fibrinogen depletion in the plasma of mice injected with siRNA LNPs after 3-months of dosing, with transferrin used as a loading control (n=3 per group). (B) Densitometric quantification of the western blot, illustrating a significant reduction in circulating fibrinogen levels. (C) Coronal brain sections were immunostained with 6E10 to detect Aβ (green) and anti-collagen IV to identify blood vessels (red) (n= 5-6 mice per group) and showed reduction in CAA upon fibrinogen depletion in TgSwDI mice. (D) Quantification of (C) showing significant decrease in CAA in the hippocampus and thalamus of siFga TgSwDI mice compared to siLuc TgSwDI mice. Scale bar= 20μm. Spatial memory of siRNA-treated mice was assessed using the Barnes maze task (n= 5-7 mice per group). During the probe trial, siFga TgSwDI mice showed a decreased latency to reach the target hole (E) and spent significantly more time around the target hole (F) compared to siLuc TgSwDI mice. Hole numbers H1, H2, etc., denote the respective hole locations, with TH indicating the target hole. Data were analyzed by using two-way ANOVA with the Bonferroni post hoc test and shown as average ± SEM; **, $P < 0.01$, ***$P < 0.001$. TH=target hole, cum duration=cumulative duration, Sec=seconds.

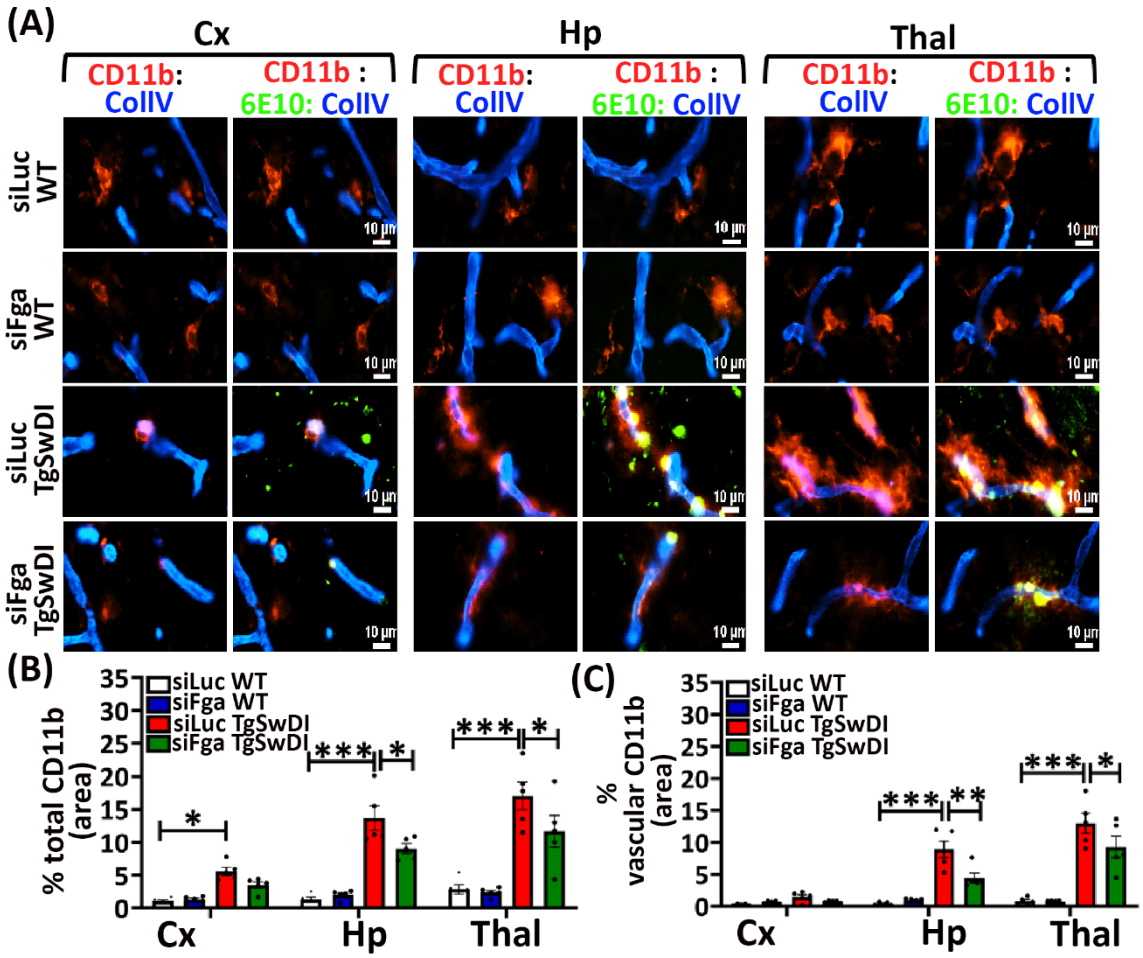


Figure 5. Fibrinogen depletion reduces microglial populations associated with CAA laden vessels in TgSwDI mice. (A) Brain sections were immunostained for CD11b (red) representing microglia, Aβ (6E10, green) and collagen IV (blue) showing decrease in microglial cells in the hippocampus and thalamus of siFga TgSwDI mice compared to siLuc TgSwDI mice. siLuc TgSwDI mice exhibited significantly higher microglial cells area compared to siLuc WT mice in cortex, hippocampus and thalamus (n=5 per group). Scale bar= 10 µm. Statistical quantification of total microglia cells (B) and microglial cells near blood vessels (vascular CD11b) (C) across cortex, hippocampus and thalamus as observed in (A). Data are expressed as mean ± SEM and analyzed using two-way ANOVA with Bonferroni post hoc test; *P < 0.05, **P < 0.01, ***P < 0.001.

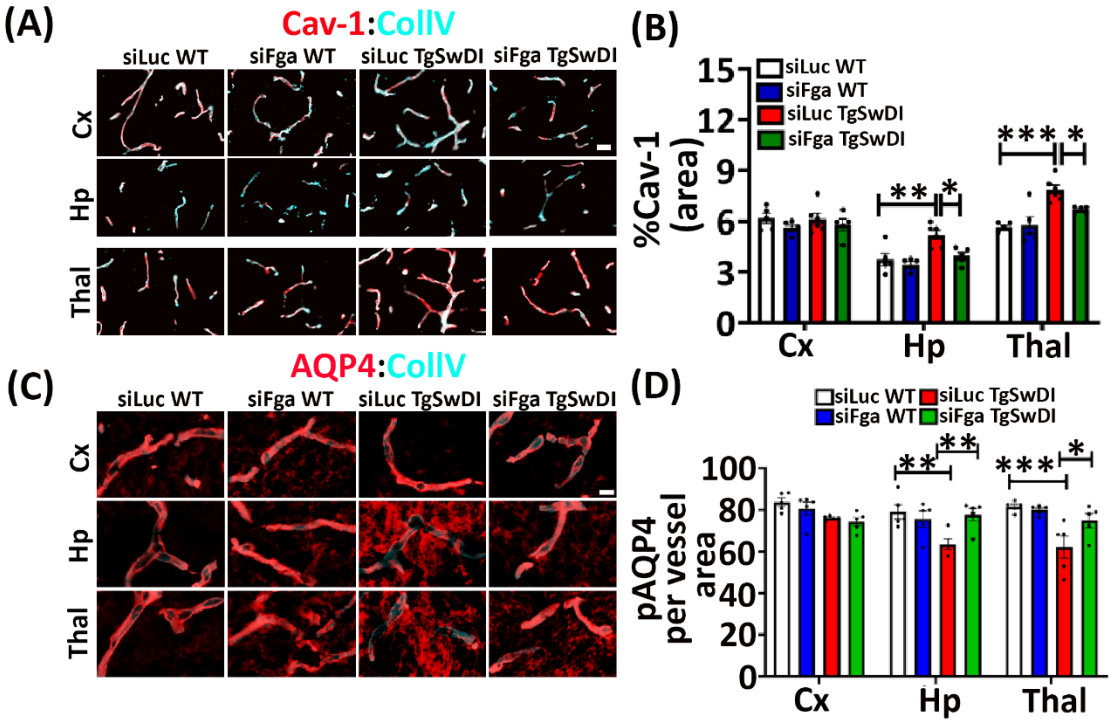


Figure 6. Fibrinogen depletion restores Cav-1 and AQP4 levels in TgSwDI mice to levels similar to those in WT littermates. (A) Brain sections were immunostained with Cav-1 (red) and CD31 (cyan). A significant decrease of Cav-1 was observed in both hippocampus and thalamus of siFga TgSwDI as compared to siLuc TgSwDI. siLuc TgSwDI mice exhibited significantly higher Cav-1 levels compared to siLuc WT mice in both the hippocampus and thalamus (n=5-6 per group). Scale bar = 20μm. (B) Statistical quantification of Cav-1 levels as observed in (A). (C) Brain sections were immunostained for AQP4 (red) and Collagen IV (cyan). A significant increase in perivascular AQP4 was found in the hippocampus and thalamus of siFga TgSwDI compared to siLuc TgSwDI. siLuc TgSwDI showed significantly lower perivascular AQP4 levels as compared to siLuc WT in both hippocampus and thalamus (n=5 per group). Scale bar= 10μm. (D) Statistical quantification of AQP4 levels as observed in (C). Data were analyzed by using two-way ANOVA with the Bonferroni post hoc test and shown as average ± SEM; *, $P < 0.05$, **, $P < 0.01$, ***$P < 0.001$.